Modelling and Testing the Stability of Edge Segments: Length and Orientation

Article · June 1996

Source: CiteSeer

CITATIONS
4

READS
22

3 authors, including:

Henrik Iskov Christensen
University of California, San Diego
512 PUBLICATIONS **8,517** CITATIONS

SEE PROFILE

Modelling and Testing the Stability of Edge Segments: Length and Orientation

Claus Brøndgaard Madsen & Henrik Iskov Christensen
Aalborg University, Fr. Bajers Vej 7D
DK-9220 Aalborg Ø, Denmark
E-mail: [cbm, hic]@vision.auc.dk

Abstract

This paper derives a model for the variance in the length and orientation of edge segments extracted from an image. It is assumed that edge pixel positions are subject to noise. The effect of this positional uncertainty is propagated all the way to segment length and orientation. The model predicts an approximately constant variance in segment length, whereas the variance in segment orientation decreases with increased segment length.

The theoretical model is verified by experiments on real images and it is shown that segment orientation is more stable (has higher signal to noise ratio) than length for segments longer than 1/10 of the image size.

1 Introduction

Edge segments extracted from images is one of the most widely used (intermediate) representations in computer vision. Edge segments are used statically for recognition and/or pose estimation from single intensity images. Dynamically, edge segments are used for as diverse purposes as structure from motion, (e.g., [8]) and control of camera motion, (e.g., [6, 9]).

While being very common in computer vision, edge segments have not been studied extensively in terms of stability. This paper addresses this issue by investigating a model for the variance in the length and the orientation of an edge segment fitted to a noisy population of edge pixels.

Obviously, modelling the noise on image derived features is a very complex matter indeed. So many parameters are involved in the imaging process, (lighting, scene contents, equipment, parameters of algorithms etc.), that it is virtually impossible to include them all into a model. This has mostly led to researchers either not addressing the problem of stability of their algorithms towards instability in edge

segments, or at best algorithms are being tested with synthetically generated edge segments perturbed with Gaussian noise of known variance.

Few references contain useful information on the expected noise level on line segment lengths and orientation. [5, 4] argue, that line segment length is inherently unreliable and base their pose estimation method solely on 'infinite' image lines determined by the position, (distance to origin), of each segment and its orientation. They test their approach for noise sensitivity using orientation noise levels of 1° and 5°, (standard deviation), respectively. They do not relate these noise levels to any experimentally obtained variances.

In an interesting paper, ([7]), the sensitivity of a pose estimation technique is modelled as a function of edge segment orientation uncertainty. The paper assumes a 5 degree error on orientations of edge segments, ($\pm$ measure). Again, this work does not present any experimentally obtained values.

The few above mentioned works represent typical ways of dealing with the problem of noise in extracted edge segments. Some theoretical work on the problem can be found in [3, 2, 1]. [3] and [2] derives covariance matrices for the parameters of infinite straight lines fitted to edge pixels, e.g., the a and b parameters in a $u + av + b = 0$ representation.

The work described in [1] addresses uncertainty problems for trinocular stereo, and does it via uncertainty on edge segment endpoints. The paper describes the transformation of a Gaussian edge pixel noise model to a covariance matrix for the coordinates of edge segment endpoints.

None of the cited works compare the theoretical considerations to noise estimations from experiments on real images. I.e., they provide no parameterization in terms of variances determined from repeatedly imaging the same scene.

This paper extends the segment endpoint uncertainty analysis presented in [1] by presenting the derivation of a orientation/length covariance matrix and the model is parameterized with experiments on real images. Sections 2 and 3 briefly summarize the results from [1]; section 4 then demonstrates how to express a model for the uncertainty in segment length and orientation due to edge pixel noise, and finally, experiments are presented that demonstrate the most important aspects of the theoretical model.

2 From edgels to an edge segment

Consider a set of paired measurements $(x_i, y_i), i = 1...n$ corresponding to the coordinates of n edge pixels as found by some edge detection process. Assume that both x and y are subject to error. Deriche et al. adopt the representation of an infinite straight line given in Eq. (1). They then demonstrate how the parameters τ and ρ can be computed from the first and second order moments of the edge pixel population to provide a least squares fit:

$$x\sin(\tau) - y\cos(\tau) + \rho \;=\; 0 \tag{1}$$

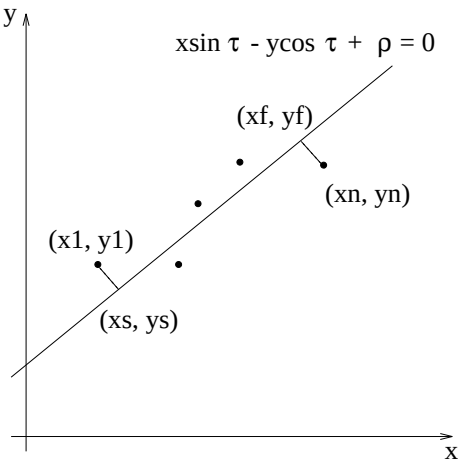

Figure 1: Fitting an edge segment to a string of edge pixels.

where

$$\bar{x} = \frac{1}{n}\sum_{i=1}^{n} x_i \qquad \bar{y} = \frac{1}{n}\sum_{i=1}^{n} y_i$$

$$a = \sum_{i=1}^{n}(x_i - \bar{x})^2 \qquad b = 2\sum_{i=1}^{n}(x_i - \bar{x})(y_i - \bar{y}) \qquad c = \sum_{i=1}^{n}(y_i - \bar{y})^2$$

$$\tau = \frac{1}{2}\arctan(\frac{b}{a-c}) \tag{2}$$

$$\rho = \bar{y}\cos(\tau) - \bar{x}\sin(\tau) \tag{3}$$

Having fitted an infinite straight line to a population of edge pixels, a line segment can be defined by projecting the extent of the population onto the fitted line. Assuming the original edge pixel population is ordered this can be achieved by projection of the first and the last pixel, (see figure 1). If $P_s(x_s, y_s)$ and $P_f(x_f, y_f)$ denote the start and finish endpoint of the segment respectively:

$$x_s = x_1 - (x_1\sin(\tau) - y_1\cos(\tau) + \rho)\sin(\tau) \tag{4}$$

$$y_s = y_1 + (x_1\sin(\tau) - y_1\cos(\tau) + \rho)\cos(\tau) \tag{5}$$

$$x_f = x_n - (x_n\sin(\tau) - y_n\cos(\tau) + \rho)\sin(\tau) \tag{6}$$

$$y_f = y_n + (x_n\sin(\tau) - y_n\cos(\tau) + \rho)\cos(\tau) \tag{7}$$

3 Covariance of edge segment end points

The infinite straight line fit by the moments is a least square error fit if the two coordinates of edge pixels have the same variance. Thus, if Σ is the covariance matrix

associated with each edge pixel, and σ_{pixel} is the standard deviation of the edge pixel coordinate noise distribution:

$$\Sigma = \begin{bmatrix} \sigma^2_{pixel} & 0 \\ 0 & \sigma^2_{pixel} \end{bmatrix} \tag{8}$$

Arguably, a non-isotropic noise model could be assumed, with different variances for each coordinate, i.e., σ^2_{xx} and σ^2_{yy}. Only, if they are not the same, the fit is no longer a least mean square error fit.

Assuming the basic edge pixel noise model represented by Eq. (8), it is possible to compute the covariance matrices of different parameters of the final segment. It can be shown, that the covariance matrix of the parameters of the infinite line, (τ and ρ), becomes:

$$\Lambda = \frac{(a+c)\sigma^2_{pixel}}{(a-c)^2+b^2} \begin{bmatrix} 1 & -d \\ -d & d^2 \end{bmatrix} + \begin{bmatrix} 0 & 0 \\ 0 & \frac{\sigma^2_{pixel}}{n} \end{bmatrix} \tag{9}$$

$$d = \bar{y}\sin(\tau) + \bar{x}\cos(\tau) \tag{10}$$

The coordinate covariance matrices of the two segment endpoints can be computed using the relations in Eqs. (4) through (7). Using the start endpoint as example, the vector $\vec{v}_s = [\ x_s \quad y_s\ ]$ expresses the endpoint coordinates as functions of the coordinates of a vector $\vec{p}_1 = [\ \tau \quad \rho \quad x_1 \quad y_1\ ]$. If Δ^s is the covariance matrix associated with the coordinates of the endpoint:

$$\Delta^s = \begin{bmatrix} \sigma^2_{x_s x_s} & \sigma^2_{x_s y_s} \\ \sigma^2_{x_s y_s} & \sigma^2_{y_s y_s} \end{bmatrix} = \frac{\partial \vec{v}_s}{\partial \vec{p}_1} \Gamma \frac{\partial \vec{v}_s}{\partial \vec{p}_1}^T \tag{11}$$

where $\partial\vec{v}_s/\partial\vec{p}_1$ is the 2×4 Jacobian matrix and Γ is the 4×4 covariance of $\vec{p}_1$:

$$\Gamma = \begin{bmatrix} & & 0 & 0 \\ & \Lambda & & \\ & & 0 & 0 \\ 0 & 0 & & \\ & & & \Sigma \\ 0 & 0 & & \end{bmatrix} \tag{12}$$

Thus, Δ^s is a 2×2 covariance matrix expressing the two variances of the 2D distribution function of endpoint coordinates. From the eigenvectors of the covariance matrix, the directions of maximum and minimum variance can be found.

4 Covariance of edge segment length and orientation

It is generally accepted that edge segment orientation is more stable than length. While the covariance matrices of the two endpoints are useful for many purposes, it

is equally important to study the uncertainties of orientation and length due to edge pixel position noise.

In order to be able to compare the variances in orientation and length signal-to-noise ratios can be studied or, equivalently, the orientation and length variables can be normalized against the respective maximum attainable values. For this study the latter approach has been chosen since it results in a more versatile formulation in terms of interpreting information from the covariance matrix.

The orientation of an edge segment has a dynamic range of π, (is modulo π), thus the maximum attainable value can be said to be $\tau_{max} = \pi$. The maximum length of an edge segment is $l_{max} = 512$ if the segment is to fall entirely within the image for any orientation, (and assuming all coordinates are in pixels). By normalizing orientation and length with these two maximum values we obtain two stochastic variables with dynamic ranges $]-0.5; 0.5[$ and $[0; 1]$ respectively:

$$\tau = (1/\tau_{max}) \arctan\left(\frac{y_f - y_s}{x_f - x_s}\right) \tag{13}$$

$$l = (1/l_{max})\sqrt{(x_f - x_s)^2 + (y_f - y_s)^2} \tag{14}$$

If we assign the coordinates of a vector $\vec{F} = [\tau, l]^T$ and $\vec{G} = [x_s, y_s, x_f, y_f]$, then the covariance $\Xi^{\tau l}$ of the vector $\vec{F}$ can be expressed as:

$$\Xi^{\tau l} = \frac{\partial \vec{F}}{\partial \vec{G}} \Upsilon \frac{\partial \vec{F}}{\partial \vec{G}}^T \tag{15}$$

where $\partial\vec{F}/\partial\vec{G}$ is the 2×4 Jacobian matrix of the orientation and length functions, and Υ is the 4×4 covariance matrix of $\vec{G}$, i.e., the endpoints. Eq. (15) expresses a first order approximation to the covariance matrix. In numerical examples we have probed the size of the second order terms against the first order terms in a Taylor expansion of both τ and l and found the second order terms to be at least two orders of magnitude smaller than the first order terms.

It can be proved, ([1]), that the correlation between one endpoint and the τ and ρ parameters of the fitted infinite line is inversely proportional to the number of edge pixels in the population. From this we justify, that zero correlation between endpoints can be assumed, and thus:

$$\Upsilon = \begin{bmatrix} & & 0 & 0 \\ & \Delta^s & & \\ & & 0 & 0 \\ 0 & & 0 & \\ & & & \Delta^f \\ 0 & & 0 & \end{bmatrix} \tag{16}$$

The Δ^s and Δ^f are computed from Eq. (11) using appropriate changes of indices for the latter of the two matrices, (the finish endpoint).

Using ordinary partial differentiation we get the elements of the Jacobian matrix of the mappings from segment endpoints to orientation and length:

$$\frac{\partial \vec{F}}{\partial \vec{G}} = \begin{bmatrix} \frac{\partial \tau}{\partial x_s} & \frac{\partial \tau}{\partial y_s} & \frac{\partial \tau}{\partial x_f} & \frac{\partial \tau}{\partial y_f} \\ \frac{\partial l}{\partial x_s} & \frac{\partial l}{\partial y_s} & \frac{\partial l}{\partial x_f} & \frac{\partial l}{\partial y_f} \end{bmatrix}$$

$$\frac{\partial \tau}{\partial x_s} = \frac{1}{\tau_{max}} \frac{y_f - y_s}{l_{max}^2 l^2} \qquad \frac{\partial \tau}{\partial y_s} = \frac{-1}{\tau_{max}} \frac{x_f - x_s}{l_{max}^2 l^2} \qquad \frac{\partial \tau}{\partial x_f} = \frac{-1}{\tau_{max}} \frac{y_f - y_s}{l_{max}^2 l^2} \qquad \frac{\partial \tau}{\partial y_f} = \frac{1}{\tau_{max}} \frac{x_f - x_s}{l_{max}^2 l^2}$$

$$\frac{\partial l}{\partial x_s} = \frac{-1}{l_{max}} \frac{x_f - x_s}{l_{max} l} \qquad \frac{\partial l}{\partial y_s} = \frac{-1}{l_{max}} \frac{y_f - y_s}{l_{max} l} \qquad \frac{\partial l}{\partial x_f} = \frac{1}{l_{max}} \frac{x_f - x_s}{l_{max} l} \qquad \frac{\partial l}{\partial y_f} = \frac{1}{l_{max}} \frac{y_f - y_s}{l_{max} l}$$

Evidently, there is a high degree of symmetry in the individual Jacobian matrix elements (apart from signs). We can therefore write the matrix as:

$$\frac{\partial \vec{F}}{\partial \vec{G}} = \begin{bmatrix} \frac{\partial \tau}{\partial x_s} & \frac{\partial \tau}{\partial y_s} & \frac{-\partial \tau}{\partial x_s} & \frac{-\partial \tau}{\partial y_s} \\ \frac{\partial l}{\partial x_s} & \frac{\partial l}{\partial y_s} & \frac{-\partial l}{\partial x_s} & \frac{-\partial l}{\partial y_s} \end{bmatrix}$$

4.1 Qualitative observations

All information required to compute the covariance matrix from Eq. (15) is present. Unfortunately, writing out the covariance matrix yields rather complex expressions. In the numerical examples below the correct approach has been used, but in favor of a behavioural characteristic an assumption shall be adopted.

The following can be noted about the covariance matrix, Υ, of the two endpoints: 1) all elements in Υ stem from the two covariance matrices Δ^s and Δ^f of the endpoints,- these are symmetric matrices and 2) the covariance matrix of the start endpoint can approximately be said to equal that of the other endpoint. Using this latter assumption:

$$\Upsilon = \begin{bmatrix} \sigma^2_{x_s x_s} & \sigma^2_{x_s y_s} & 0 & 0 \\ \sigma^2_{x_s y_s} & \sigma^2_{y_s y_s} & 0 & 0 \\ 0 & 0 & \sigma^2_{x_s x_s} & \sigma^2_{x_s y_s} \\ 0 & 0 & \sigma^2_{x_s y_s} & \sigma^2_{y_s y_s} \end{bmatrix} \tag{17}$$

It is now possible to compute a tractable expression for the covariance between orientation and length. From Eq. (15):

$$\begin{aligned} \Xi^{\tau l} &= \begin{bmatrix} \frac{\partial \tau}{\partial x_s} & \frac{\partial \tau}{\partial y_s} & \frac{-\partial \tau}{\partial x_s} & \frac{-\partial \tau}{\partial y_s} \\ \frac{\partial l}{\partial x_s} & \frac{\partial l}{\partial y_s} & \frac{-\partial l}{\partial x_s} & \frac{-\partial l}{\partial y_s} \end{bmatrix} \begin{bmatrix} \sigma^2_{x_s x_s} & \sigma^2_{x_s y_s} & 0 & 0 \\ \sigma^2_{x_s y_s} & \sigma^2_{y_s y_s} & 0 & 0 \\ 0 & 0 & \sigma^2_{x_s x_s} & \sigma^2_{x_s y_s} \\ 0 & 0 & \sigma^2_{x_s y_s} & \sigma^2_{y_s y_s} \end{bmatrix} \begin{bmatrix} \frac{\partial \tau}{\partial x_s} & \frac{\partial l}{\partial x_s} \\ \frac{\partial \tau}{\partial y_s} & \frac{\partial l}{\partial y_s} \\ \frac{-\partial \tau}{\partial x_s} & \frac{-\partial l}{\partial x_s} \\ \frac{-\partial \tau}{\partial y_s} & \frac{-\partial l}{\partial y_s} \end{bmatrix} \\ &= \begin{bmatrix} \sigma^2_{\tau\tau} & \sigma^2_{\tau l} \\ \sigma^2_{\tau l} & \sigma^2_{ll} \end{bmatrix} \end{aligned} \tag{18}$$

$$\sigma^2_{\tau\tau} = 2\frac{(y_f-y_s)^2\sigma^2_{x_sx_s} - 2(x_f-x_s)(y_f-y_s)\sigma^2_{x_sy_s} + (x_f-x_s)^2\sigma^2_{y_sy_s}}{\tau^2_{max}l^4_{max}l^4} \quad (19)$$

$$\sigma^2_{\tau l} = 2\frac{(x_f-x_s)(y_f-y_s)(\sigma^2_{y_sy_s} - \sigma^2_{x_sx_s}) + ((x_f-x_s)^2 - (y_f-y_s)^2)\sigma^2_{x_sy_s}}{\tau_{max}l^4_{max}l^3} \quad (20)$$

$$\sigma^2_{ll} = 2\frac{(x_f-x_s)^2\sigma^2_{x_sx_s} + 2(x_f-x_s)(y_f-y_s)\sigma^2_{x_sy_s} + (y_f-y_s)^2\sigma^2_{y_sy_s}}{l^4_{max}l^2} \quad (21)$$

It requires considerable insight to foresee the relative sizes of the elements in the covariance matrix for orientation and length as presented in Eqs. (18) through (21). Using some simplifications and studying the expressions the following observations can be made, (using rough estimates on the parameters in the expressions):

- The two off-diagonal elements of $\Xi^{\tau l}$, representing the covariance of orientation and length of a segment, are very small compared to the diagonal elements, i.e., the pure variances. An effect of this is that the ellipses of uncertainty will have major and minor axes that are almost parallel to the coordinate axes in an orientation-length coordinate system.

- It can also be noted that the variance in orientation, $\sigma^2_{\tau\tau}$ can be expected to be smaller than the variance in length σ^2_{ll}, i.e., orientation is a less noisy signal.

- Finally, it can be noted that the variance in orientation depends upon the length in a such a way that the variance increases for a decrease in length. This in intuitively obvious since a segment with support from very few edge pixel will be less stable than a segment extending through the entire image.

The simplest way to get an rough overview of these aspects is to assume that only two edge pixels are used to form the segment, namely the first and last. I.e., the segment is determined directly by the two endpoints, which will then only be subject to edge pixel noise with covariance Σ. In this case $\sigma^2_{x_sx_s} = \sigma^2_{y_sy_s}$ and $\sigma_{x_sy_s} \equiv 0$.

5 Experimental verification

Given a covariance matrix $\Xi^{\tau l}$ associated with and computed for some specific segment, we can use the squared Mahalanobis distance to form an ellipse of uncertainty around the measurement. That is, if τ_0 and l_0 are the orientation and length of some *specific* segment, then the equation:

$$(\tau-\tau_0, l-l_0)(\Xi^{\tau l})^{-1}(\tau-\tau_0, l-l_0)^T = k^2 \quad (22)$$

expresses an elliptic area within which, statistically, some percentage of the orientation/length measurements would fall if the measurements were repeated over a large number of images of the same edge segment on the same object. The k^2 value can

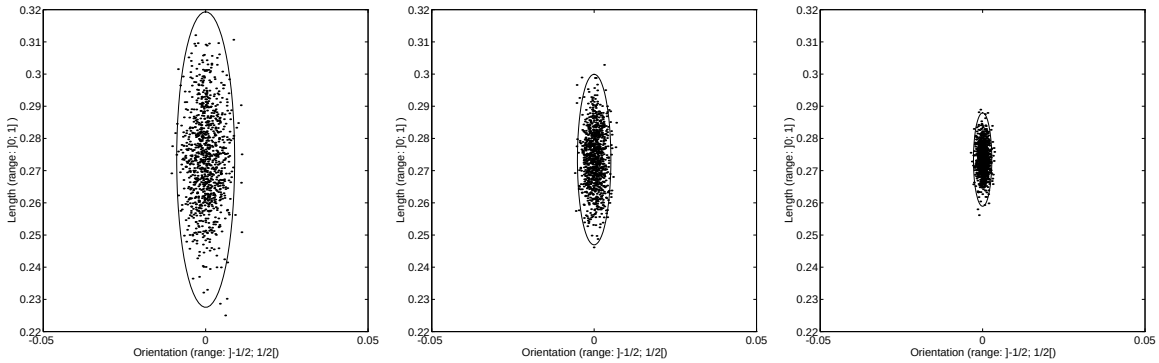

Figure 2: Three plots showing orientation and length computed for the same ideal edge pixel population added three different levels of Gaussian noise to coordinates. For all plots the uncertainty ellipse was computed using $k^2 = 9.21$ for a theoretical percentage of measurements being inside of 99%. The used noise levels were $\sigma^2_{pixel} =$ 30, 10 and 3, (pixels). For each plot 1000 noisy versions of the original population were computed. The percentages of measurements inside the uncertainty ellipses were 98.0, 97.2 and 97.5 respectively.

be looked up in a χ^2 distribution table, (using 2 degrees of freedom); e.g., for a probability of 95% a value of $k^2 = 5.99$ should be used.

In the figures to be shown subsequently, these ellipses will be included since they effectively present what is predicted by the theoretical noise model.

5.1 Synthetic data

As mentioned previously a first order approximation to the Taylor series expansion of the function mapping segment endpoints to orientation and length was used, (Eq. (15)). To test the validity of this approximation, we can, in accordance with the basic edge pixel noise model, add known Gaussian noise to an ideal population of edge pixels, and hold the number of measurements that fall inside the ellipse of uncertainty up against the percentage predicted by the χ^2 table.

A number of such experiments have been performed, the results of some are illustrated in figure 2. Also, tables 1 through 3 give a more accurate impression of the performance of the orientation/length noise model in terms of predicting the number of samples being within some distance of the mean.

The presented tables show, that the derived covariance model for orientation and length tends to underestimate the variances slightly. There is a systematic tendency when comparing to the percentages predicted by the χ^2 table. Yet, it can be noted that for varying k^2 the model follows what is predicted. The minor quantitative discrepancy between model and prediction must be attributed to the first order approximations made in computing the covariance matrix for orientation versus length.

Still, as seen from figure 2 there is a good qualitative accordance between the

Table 1: An ideal population of edge pixels has been perturbed with Gaussian noise of different variance, as indicated by σ^2 above the three rightmost columns. The segment lengths and orientations have been computed for each of 1000 noisy version of the original population. The percentage of orientation/length measurement falling inside the ellipse of uncertainty (as determined by the presented noise model) is in the table compared to the percentage predicted by the χ^2 table, (leftmost column). This has been done for varying k^2 parameters, (larger k^2 means larger percentage of noisy measurements falling inside ellipse).

$l_0 = 0.1353$

	$\sigma^2 = 1.0$	$\sigma^2 = 3.0$	$\sigma^2 = 6.0$
$\mathcal{P}$	%	%	%
50%	41.6%	39.8%	43.6%
80%	71.7%	70.3%	72.6%
90%	83.3%	83.6%	83.8%
95%	89.5%	90.4%	90.1%

Table 2: The same type of table as 1, only for a longer segment.

$l_0 = 0.2735$

	$\sigma^2 = 1.0$	$\sigma^2 = 3.0$	$\sigma^2 = 6.0$
$\mathcal{P}$	%	%	%
50%	45.4%	42.8%	39.3%
80%	71.8%	75.8%	72.7%
90%	84.1%	85.9%	83.2%
95%	90.6%	90.0%	91.8%

Table 3: As previous two tables.

$l_0 = 0.5497$

	$\sigma^2 = 1.0$	$\sigma^2 = 3.0$	$\sigma^2 = 6.0$
$\mathcal{P}$	%	%	%
50%	43.8%	42.0%	43.0%
80%	70.0%	73.0%	71.1%
90%	81.6%	82.3%	84.4%
95%	90.4%	90.7%	89.9%

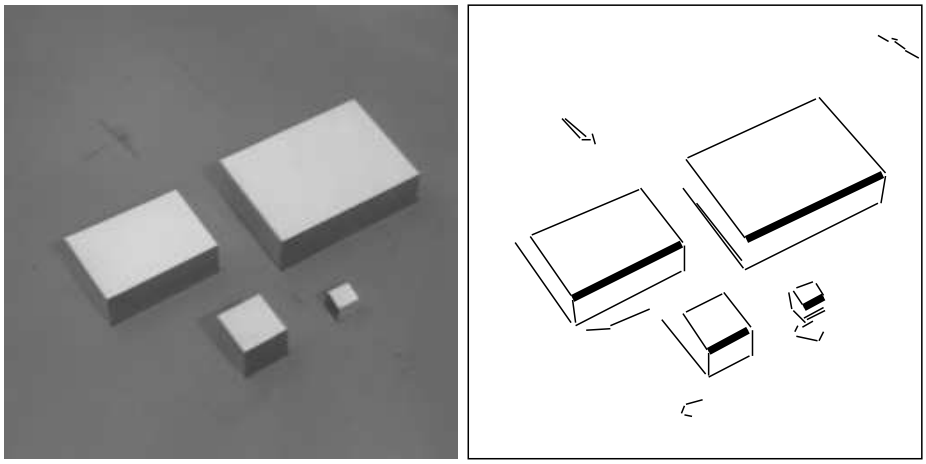

Figure 3: Image and extracted line segments used in experiment. The front most edge of each object was tracked through a sequence of 200 images.

scatter predicted by the model (the ellipses), and the actual scatter of the measurements. This indicates that the relative sizes of the orientation and length variances are correct.

5.2 Real data

As stated previously the orientation/length noise model predicts that the variance in orientation should decrease with increasing segment length. To test this, a scene of simple polyhedra was imaged 200 times keeping lighting constant and the normalized orientation and length was computed for four segments of different lengths, (figure 3).

The conditions under which the experiments were performed were similar to those of a typical table-top computer vision system. The objects were made of colored cardboard aligning sharply at edges and the distance from camera to object was approximately 1 m. A Canny edge detector was used to produce chains of edge pixels and segments were produced using the fitting described in section 2.

All the data points from the 200 images including the uncertainty ellipses are plotted in figures 4. Figure 4 clearly demonstrate the ability of the noise model to describe the perturbations experienced when repeatedly imaging the same edge segment. Even if the effects of quantization are evident, (the 200 measurements for each of the four segment fall in only a few discrete data points), the scatter is well captured by the appearance of the uncertainty ellipses. Thus qualitatively, the model is in good accordance with reality.

The ellipses in figure 4 correspond to the squared Mahalanobis distance within which 95% of the measurements should fall according to a χ^2 distribution table. The noise model for orientation and length represented by Eq. (15) has one 'free' parameter: the edge pixel coordinate variance σ^2_{pixel}. By adjusting this parameter

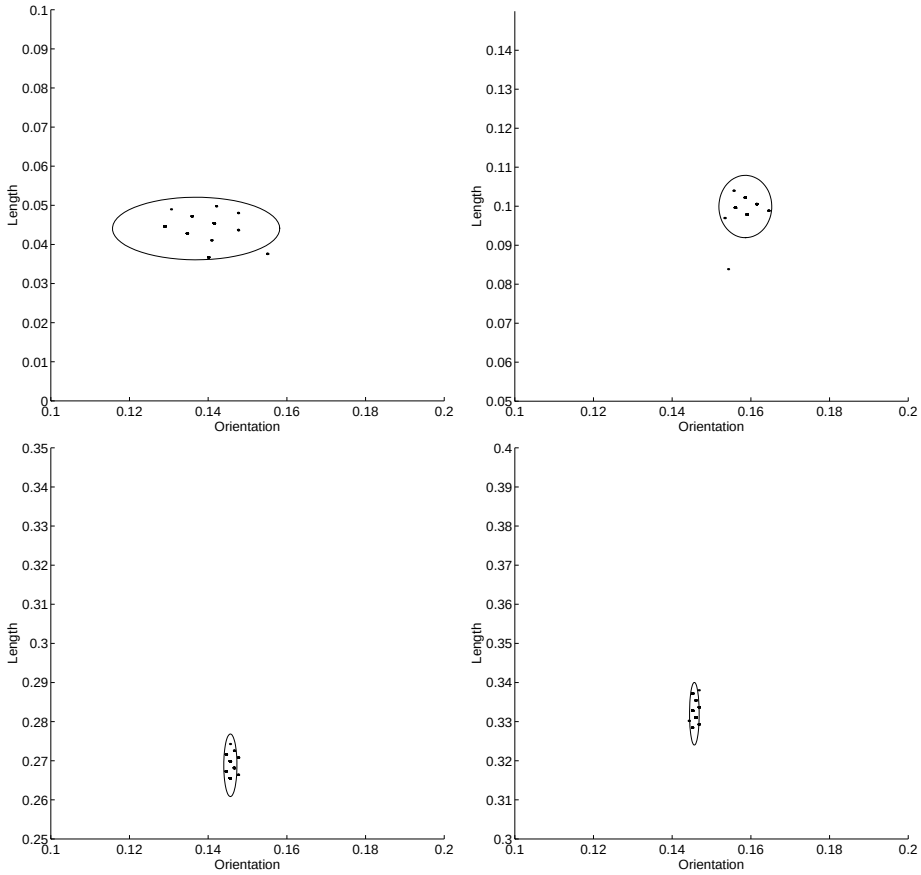

Figure 4: Orientation and length data points for 4 line segments over a sequence of 200 images. Each plot corresponds to a segment, (top left: shortest segment, bottom right: longest segment),- all plots are to the same scale and can be compared directly, (only starting point on length axis varies). Notice the ability of the uncertainty ellipses, (computed analytically), to capture the characteristics of the scatter.

it is possible to find a value for which the frequency of data points falling inside ellipses corresponds approximately to the percentages predicted by a table. In the experiments reported here a σ^2_{pixel} value of 1.4 pixels gave best quantitative results, (table 4). It is seen that the relatively low number of data points for each segment as well as the quantization effect makes it hard to get good quantitative performance of the model for very short segments. For longer segment the model performs quite well in terms of predicting the numerical orientation and length variances.

Table 5 presents some crucial characteristics of the data points for each of the four segments. It readily seen that the variance is more or less constant with varying length, whereas the variance in orientation decreases drastically with increasing segment length. For a segment of 0.1 times the image width, i.e., approximately 50 pixel long, the variance in orientation is on the same order as the variance in length. For longer segments, the variance is much smaller. A segment length of one third of

Table 4: Computed versus predicted percentage of orientation/length measurements inside some distance from mean, left column is theoretical values.

Orientation/length, $\sigma^2_{pixel} = 1.4$

	Segment number			
	1	2	3	4
$\mathcal{P}$	%	%	%	%
50%	86.0%	95.0%	50.0%	62.5%
80%	91.0%	96.0%	78.0%	76.0%
90%	92.5%	97.0%	92.5%	86.0%
95%	98.0%	99.5%	92.5%	98.0%

Table 5: Notice how, when length decreases, the variance in orientation increases, while variance in length is almost constant. The outlier measurement setting a very low minimum value for the length of segment 4 causes the variance to be higher than what is actually reasonable. Note: length and orientation are normalized values and thus the standard deviations can be compared directly. A normalized orientation standard deviation of $1 \cdot 10^{-3}$ corresponds to $0.18°$.

Length

	mean	std. dev.	min	max
Segment 1	0.0441	$2.52 \cdot 10^{-3}$	0.0367	0.0448
Segment 2	0.0999	$1.93 \cdot 10^{-3}$	0.0839	0.1040
Segment 3	0.2688	$2.24 \cdot 10^{-3}$	0.2655	0.2743
Segment 4	0.3320	$7.11 \cdot 10^{-3}$	0.2376	0.3380

Orientation

	mean	std. dev.	min	max
Segment 1	0.1369	$6.04 \cdot 10^{-3}$	0.1289	0.1550
Segment 2	0.1586	$2.30 \cdot 10^{-3}$	0.1533	0.1645
Segment 3	0.1456	$0.87 \cdot 10^{-3}$	0.1445	0.1476
Segment 4	0.1456	$0.59 \cdot 10^{-3}$	0.1442	0.1468

the image width can be expected to have almost 20 times lower variance in orientation than in length, (note: the tables list standard deviations). A normalized orientation standard deviation of $1 \cdot 10^{-3}$ corresponds to a standard deviation of 0.18 degrees.

Thus, the behaviour predicted by the model in terms of the dependency between segment length and orientation variance is substantiated by the experiments.

Another 200 images of the scene in figure 3 was acquired, only the focal length of the camera was increased so that the lengths of the two shortest segments increased by a factor of 5, (bringing them to have comparable length to the two longer segments in the first set of images). This zooming reduced the orientation variances of the two short segments from $6.04 \cdot 10^{-3}$ and $2.30 \cdot 10^{-3}$ to $0.77 \cdot 10^{-3}$ and $0.54 \cdot 10^{-3}$ respectively. The variances in length were largely unchanged.

This shows that zooming can be performed to increase segment length and thereby to increase orientation stability. This observation is important and should be exploited in active vision techniques using motorized lenses.

6 Conclusion

The paper presented an analytical model of the instability in edge segment length and orientation. The model is based on assuming a simple uncertainty model for the position of individual edge pixels and propagates the effects of this to the length and orientation of an edge segment fitted to a population of edge pixels.

The paper also actually tested the model against results obtained from real images by imaging the same scene repeatedly and computing lengths and orientations for selected edge segments. The experiments demonstrated the ability of the model to predict the distribution in the orientation/length measurements of segments.

Also, the experiments verified the most important characteristics of the analytical model: 1) the stability of segment orientation increases with increasing segment length, and 2) even for segments of modest length orientation measurements have a higher signal-to-noise ration than length measurements.

In conclusion the paper effectively demonstrates, both theoretically and experimentally, that edge segment orientation is a more robust feature than segment length.

7 Acknowledgements

The authors gratefully acknowledge funding by the Danish Technical Research Council under the MOBS Framework programme, and by the EU ESPRIT Basic Research Action BR 3038/7108, Vision As Process.

References

[1] R. Deriche, R. Vaillant, and O. Faugeras. From noisy edge points to 3d reconstruction of a scene: A robust approach and its uncertainty analysis. In *Proceedings: Seventh Scandinavian Conference on Image Analysis, Aalborg, Denmark*, pages 225 – 232, August 1991.

[2] O. Faugeras. *Three-Dimensional Computer Vision - A Geometric Viewpoint*. MIT Press, Cambridge, Massachusetts, 1993.

[3] K. Kanatani. *Geometric Computation for Machine Vision*. Oxford Science Publications. Clarendon Press, Oxford, UK., 1993.

[4] R. Kumar and A. R. Hanson. Robust estimation of camera location and orientation from noisy data with outliers. In *Proceedings: IEEE Workshop on Interpretation of 3D Scenes, Austin, Texas*, November 1989.

[5] Rakesh Kumar. *Model Dependent Inference of 3D Information from A Sequence of 2D Images*. PhD thesis, Department of Computer and Information Science, University of Massachusetts at Amherst, February 1992. Tech rep. no. COINS TR92-04.

[6] C. B. Madsen and H. I Christensen. Reactive view planning for quantification of local geometry. In *Proceedings: IEEE Conference on Computer Vision and Pattern Recognition, Seattle, Washington*, pages 823 – 828, June 1994.

[7] J.L. Mundy, A.J. Heller, and D.W. Thompson. The concept of an effective view point. In *Proceedings: DARPA Image Understanding Workshop*, pages 651 – 659, April 1988.

[8] D. W. Murray, D. A. Castelow, and B. F. Buxton. From image sequences to recognized moving polyhedral objects. *International Journal of Computer Vision*, (3):181 – 208, 1989.

[9] D. Wilkes and J.K. Tsotsos. Integration of camera motion behaviours for active object recognition. In *Proceedings: IEEE Workshop on Visual Behaviours in conjunction with the IEEE Conference on Computer Vision and Pattern Recognition, Seattle, Washington*, pages 10 – 19, June 1994.